Jurnal Polimesin
Department of Mechanical Engineering
State Polytechnic of Lhokseumawe
http://e-jurnal.pnl.ac.id/polimesin
e-ISSN : 2549-1999 No. : 6 Month : December
p-ISSN : 1693-5462 Volume : 23 Year : 2025

Processing dates: received on 2025-09-05, reviewed on 2025-11-23, accepted on 2025-12-04 and online availability on 2025-12-31

Numerical investigation of heat reduction system in 42110 Lithium-Ion battery packs using cooling plate spacing variations

Bima Rakha Adhitama[1], James Julian[1*], Fitri Wahyuni[1], Fathin Muhammad Mahdhudhu[2], Elvi Armadani[3]
[1]Department of Mechanical Engineering, Faculty of Engineering, Universitas Pembangunan Nasional Veteran Jakarta, Jakarta 12450, Indonesia
[2]Department of Naval Architecture, Faculty of Engineering, Universitas Pembangunan Nasional Veteran Jakarta, Jakarta 12450, Indonesia
[3]Department of Industrial Engineering, Faculty of Engineering, Universitas Pembangunan Nasional Veteran Jakarta, Jakarta 12450, Indonesia
*Corresponding Author: zames@upnvj.ac.id

Abstract
An efficient thermal reduction system is crucial for ensuring the optimal performance and safety of Electric Vehicle (EV) batteries, notably by maintaining uniform temperature distribution and minimizing the risk of thermal runaway. This study presents a numerical investigation of the thermal behaviour of a liquid-cooled system for a cylindrical Li-ion 42110 battery pack, focusing on the influence of varying cold-plate spacing. Three cold plate configurations with spacing ratios r = 0.78, r = 0.33, and r = 0 were examined, with r = 0.78 corresponding to the most significant separation. The simulation employed a Reynolds-Averaged Navier–Stokes (RANS) model to resolve fluid flow and energy transport, and the heat-generation profile was derived from experimental data. The results show that all cooling configurations substantially reduced the maximum temperature relative to the uncooled case, with the widest spacing (r = 0.78) achieving the most significant average reduction of 19.736%. However, designs with smaller spacing exhibited slightly higher temperatures and reduced uniformity, particularly near the positive pole, where heat concentration is more pronounced. The temperature deviation remained within the acceptable 2% threshold. These findings highlight not only the thermal effectiveness of each spacing ratio but also its design implications, demonstrating that spacing plays a critical role in controlling peak temperature and maintaining uniformity. Overall, the study emphasizes that strategic cold-plate spacing is essential for reliable, efficient, and thermally stable battery operation in EV applications.

Keywords:
EVs, Li-ion battery, thermal reduction, cooling system

1 Introduction

The transition to clean, sustainable energy is a crucial step in addressing global climate change and the non-renewable nature of fossil fuels. In this sense, the transport sector holds a key position due to its direct contribution to total greenhouse gas emissions [1]. Electric Vehicles (EVs) are increasingly a game-changer and a promising solution with enormous potential to decrease carbon footprints and to mitigate urban air quality. The EV transition is also directly aligned with Sustainable Development Goal (SDG) 7, which emphasizes affordable, reliable, sustainable, and modern energy for all. With the increasing popularity of EVs, the need for effective and reliable energy sources, such as lithium-ion (Li-ion) batteries [2], is becoming increasingly urgent. Li-ion batteries are the dominant energy storage devices for EVs, primarily due to their excellent energy and power density and cycle life [3]. However, the performance and lifespan of a Li-ion battery are significantly temperature-dependent [4]. During charging and discharging, batteries generate significant internal heat. This thermal buildup, in turn, will result in a nonuniform temperature distribution around the cell, causing serious issues such as thermal runaway [5]. Therefore, maintaining battery temperatures within a safe operating range (20−40°C) and ensuring temperature uniformity across the module, which is a primary issue in Li-ion batteries, are crucial challenges in EV Development [6]. Various approaches have been explored for managing thermal management in batteries, including air cooling. Despite their ability to reduce battery temperature, air-cooling methods, as investigated by Mohamed Kh Saudi et al. through variations in spacing and fins, have proven suboptimal at achieving significant temperature reduction for Li-ion batteries and have negatively affected the pack size by 69% [7]. In contrast, another approach to cooling using Phase Change Material (PCM) cooling has been conducted by Vivek Saxena *et al.*, who found that the temperature produced by the battery can be reduced effectively, despite the PCM being unable to maintain its cooling performance at high ambient temperatures and high discharge rates [8]. Another approach, using a phase-change composite thin film, was also investigated by Se Won Kim *et al.* [9]. The use of PCM thin film primarily aims to improve cell compactness. Although the overall cell size was significantly reduced, these passive methods generally lack the capacity to manage rapid thermal fluctuations under high-power EV operation.

The approach using passive cooling methods, as discussed previously, has proven to be inefficient. An active cooling method was investigated by Soner Birinci *et al.* [10], who evaluated both maximum temperature and inhomogeneity. However, this method employed various inlet flow rates up to 0.01 kg/s without accounting for pump power consumption. Furthermore, Zhonghao Rao *et al.* [11] investigated the thermal performance of liquid-cooled cylindrical lithium-ion battery modules, specifically examining the effect of variable contact surfaces on temperature uniformity. Among these options, active liquid-based cooling systems show significant potential for high-power battery applications due to their superior heat-transfer capabilities and ability to reduce temperature. Despite these advancements, the influence of cooling on both temperature reduction and uniformity in cylindrical battery modules remains insufficiently understood. Nevertheless, the optimal design of cooling, particularly for cylindrical battery modules, requires careful consideration of geometry and the structural complexity of cooling-channel configurations to achieve maximum temperature reduction [12,13]. Therefore, this study presents a systematic evaluation of cold-plate spacing ratios in an active liquid-cooled system for cylindrical 42110 Li-ion battery packs. The novelty of this work lies in introducing the spacing ratio as a geometric design parameter, quantitatively assessing its impact on both heat reduction and thermal uniformity, and providing an optimized spacing configuration that balances cooling performance and stability while accounting for other limitations. Furthermore, an optimal design for the liquid cooling system is presented, showing both heat reduction and power consumption.

2 Research methodology

2.1 Geometry of the models

Battery packs in EVs are typically comprised of numerous battery cells. For this study, a 42110 Li-ion battery module featured eight cylindrical cells arranged along a flow channel. The core of the liquid cooling system employed in this research utilizes

aluminum blocks positioned between the cells. Within these aluminum blocks, an 8 mm channel is integrated to facilitate water flow. Crucially, maintaining a uniform temperature distribution across the battery module is paramount to its longevity and safety, as it avoids localized heat-generating areas that compromise overall efficiency. To thoroughly investigate the impact of cold plate configuration on thermal performance, three distinct cold plate designs were developed, each varying in cooling-channel spacing, as shown in Fig. 1. These designs are systematically represented with ratios explained in Table 1, as illustrated in Fig. 2. In this study, the spacing ratio r is defined as a dimensionless parameter that quantifies the normalized distance between adjacent cooling channels. It is calculated using Eq. (1), where s denotes the spacing between batteries, d the minimum spacing, and l the maximum spacing. Thus, the selected values r = 0, r = 0.33, and r = 0.78 correspond to different spacing configurations, enabling a systematic comparison of thermal behavior across different spacing arrangements.

$$r = \frac{d}{l} \tag{1}$$

Table 1. Variations of the spacing

Models	*s*	*r*
1		0.78
2	*s* = 10 *mm*	0.33
3		0

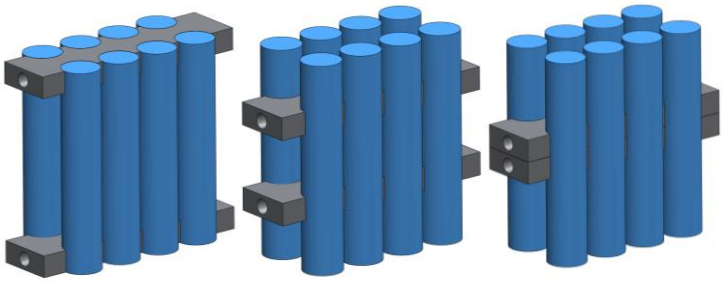

(a) (b) (c)

Fig. 1. Cooling plate spacing ratios: (a) *r* = 0.78, (b) *r* = 0.33, (c) *r* = 0

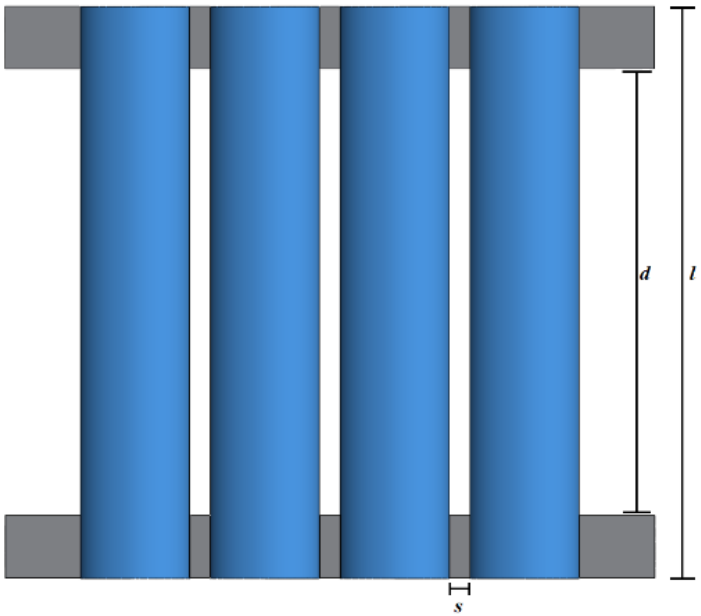

Fig. 2. Schematic representation of the battery module and cooling plate configuration

2.2 Governing Equations

To analyze the thermal–fluid behavior of the cooling system, this study applies the Reynolds-Averaged Navier–Stokes (RANS) equations together with an energy conservation model, with the spacing ratio r, defined in Eq. (1), as a nondimensional measure of channel spacing. The continuity and momentum equations govern coolant flow (Eqs. (2) and (3)) and capture mass conservation and viscous flow behavior [12]. In contrast, the temperature field in both the coolant and battery domains is governed by the energy equation (Eq. (4)), which includes conduction, convection, and volumetric heat generation [13,14]. The heat source term is obtained from experimental discharge data as shown in Eq. (5) [15], and further formulated into a transient parametric model in Eq. (6) to account for spatially nonuniform and time-dependent thermal effects during high-rate discharge [16].

$$\frac{\partial \rho}{\partial t} + \frac{\partial}{\partial x_i}(\rho u_i) = 0 \tag{2}$$

$$\frac{\partial}{\partial t}(\rho u_i) + \frac{\partial}{\partial x_i}(\rho u_i u_j) = \frac{\partial p}{\partial x_i} + \frac{\partial}{\partial x_j}\left[\mu\left(\frac{\partial u_i}{\partial x_j} + \frac{\partial u_j}{\partial x_i} - \frac{2}{3}\delta_{ij}\frac{\partial u_i}{\partial x_i}\right)\right] + \frac{\partial}{\partial x_i}\left(-\rho\overline{u_i' u_j'}\right) \tag{3}$$

$$\rho c_p \frac{\partial T}{\partial t} = \lambda_x \frac{\partial^2 T}{\partial^2 x} + \lambda y \frac{\partial^2 T}{\partial^2 y} + \lambda z \frac{\partial^2 T}{\partial^2 z} + Q_{gen} \tag{4}$$

$$Q_{gen}(t) = \rho c_p \frac{\Delta T}{\Delta t} \tag{5}$$

$$Q_{gen(1-3)}(x,y,z,t) = Q_{gen(1-3)}(t) - \lambda \nabla^2 T_{(1-3)} \tag{6}$$

2.3 Mesh and boundary conditions

To effectively simulate complex geometry, particularly the channels and the cells, the computational domain was discretized using an unstructured tetrahedral mesh. This approach is advantageous because it provides flexibility to model the mesh in regions surrounding the cells accurately. Fig. 3 shows a schematic of the boundary setup, while Fig. 4 shows the mesh representation. The system consists of cylindrical cells encased in an aluminum block that contains a channel for liquid coolant. The inlet velocity was set to 0.0005 kg/s to account for power consumption. The velocity inlet was specified as the boundary condition. On the inner surface of the channel, a no-slip condition was applied, and the entire pack was treated as adiabatic, with an inlet temperature of 25°C. The material properties used in the simulation are listed in Table 2.

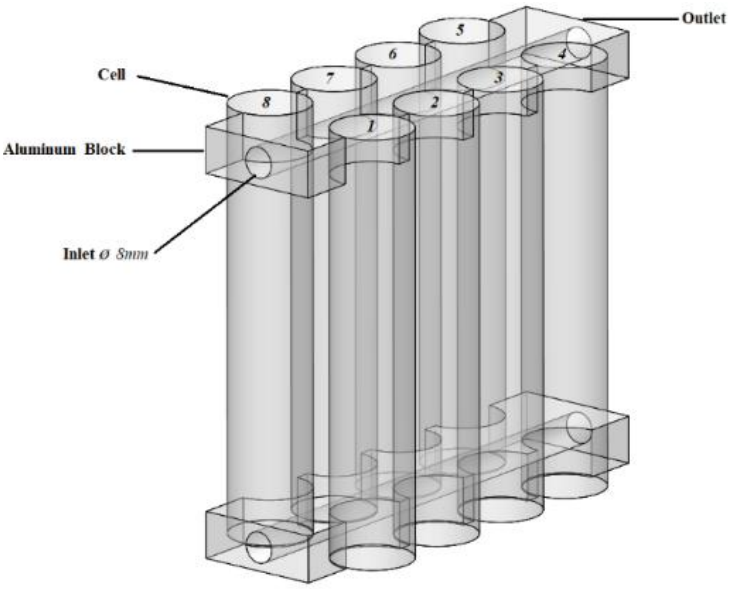

Fig. 3. Boundary condition configuration for the liquid-cooled battery module

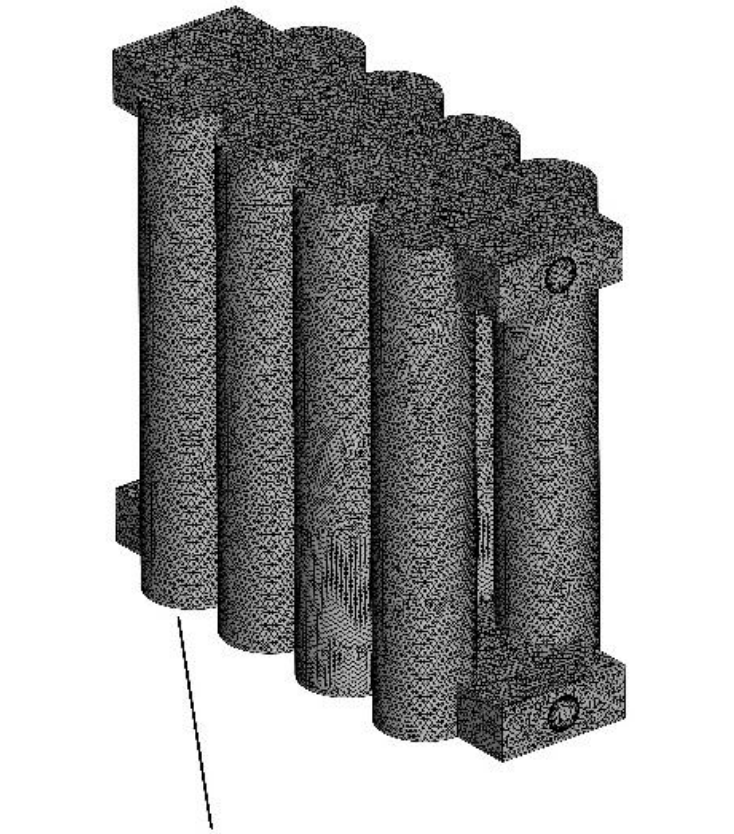

Fig. 4. Mesh visualization of the battery module

Table 2. Material properties

Materials	ρ ($kg \cdot m^{-3}$)	C ($J \cdot kg^{-1} \cdot k^{-1}$)	k ($W \cdot m^{-1} \cdot k^{-1}$)	μ ($g \cdot m^{-1} \cdot s^{-1}$)
Aluminum	2719	871	202.4	-
Battery	2450	1108.4	3.917	-
Water	998.2	4128	0.6	1.003

2.4 Grid independence test

The mesh quality employed in Computational Fluid Dynamics simulations affects the accuracy of the results. A grid-independence test is conducted to determine the optimal mesh count across various mesh variants, thereby ensuring the accuracy of the results. The coarse mesh yields elements of 1,555E+06, the medium mesh yields elements of 2,333E+06, and the fine mesh yields elements of 3,5E+06. The methodology used in this study is based on the Richardson extrapolation technique, as generalized by Roache [17]. Eqs. (9) and (10) are used to estimate the error value of each coarse and fine mesh. The mesh independence test was also conducted with a safety factor of 1.25, yielding a minimum relative error (Table 3), indicating that mesh changes affect the convergence index. Fig. 5 demonstrates that finer meshing yields a more accurate estimate of the desired value. This leads to the selection of a fine mesh for further computations.

$$r = \frac{h_2}{h_1} \tag{7}$$

$$\bar{p} = \frac{\ln\left(\frac{f_3 - f_2}{f_2 - f_1}\right)}{\ln(r)} \tag{8}$$

$$GCI_{fine} = \frac{F_s \,|\epsilon|}{\left(r^{\bar{p}} - 1\right)} \tag{9}$$

$$GCI_{coarse} = \frac{F_s \,|\epsilon|\, r^{\bar{p}}}{\left(r^{\bar{p}} - 1\right)} \tag{10}$$

$$\epsilon = \frac{f_{n+1} - f_n}{f_n} \tag{11}$$

$$\frac{GCI_{coarse}}{GCI_{fine} r^{\bar{p}}} \approx 1 \tag{12}$$

$$f\,r_{h=0} = f_1 + \frac{(f_1 - f_2)}{\left(r^{\bar{p}} - 1\right)} \tag{13}$$

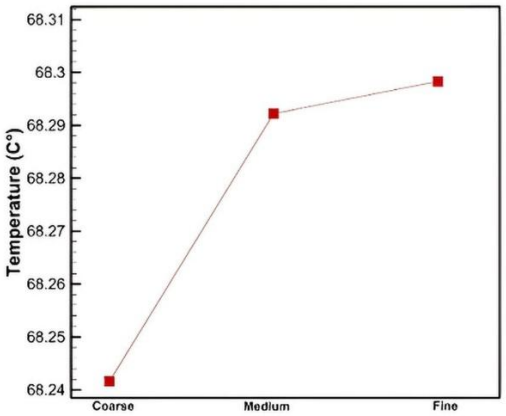

Fig. 5. Mesh sensitivity

Table 3. Results of the grid convergence index (GCI)

Mesh		Fine	Medium	Coarse
Difference in temperature		68.2983	68.2922	68.24165
$\bar{\bar{p}}$			5.215428238	
R			1.5	
GCI_{fine}			0.002%	
GCI_{coarse}			0.0127%	
$f_{rh}=0$			68.29914	
$\frac{GCI_{coarse}}{GCI_{fine} r^{\bar{p}}}$			1	
Error	T	0.00123%	0.01016%	0.08417%

3 Results and discussion

3.1 Validation

The experimental data consisted of the three heat-source values, and the experimental setup was conducted using this method because the chemical reaction at the positive terminal is slightly larger than in other areas. The main idea is to capture vertical inhomogeneity within the battery. The experiment was conducted by Zhonghao *et al*. [18] at a 5 °C discharge rate, which represents high-power operating conditions in which thermal effects are more pronounced and critical for evaluating battery performance. Fig. 6 shows the similarity between the computed and experimental results, with an error of 3.99%, indicating the validity of the battery heat-generation model in the simulation.

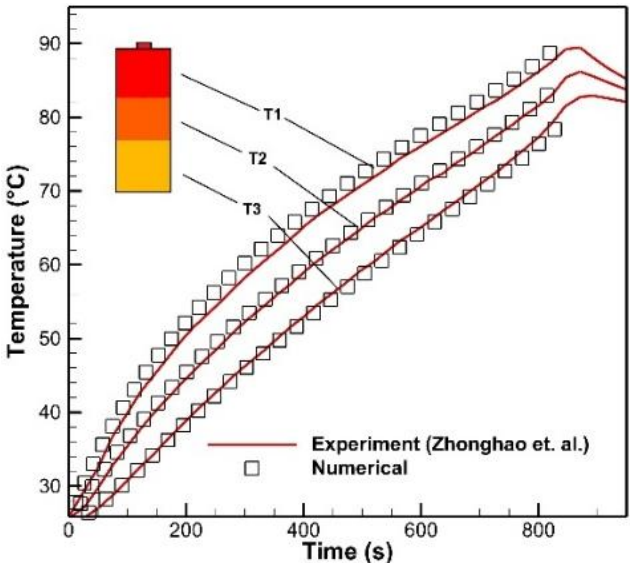

Fig. 6. Comparison between numerical and experimental

3.2 Analysis

3.2.1 Average temperature distribution

Fig. 7 presents a detailed representation of the heat generated within each battery cell. The values shown are the average temperatures for each cell, enabling a clear comparison of their thermal behaviour across three distinct spacing ratios: r = 0.78, r = 0.33, and r = 0. As illustrated in the figure, a similar temperature pattern is observed between opposing cells such as (cell 1,8), (cell 2,7), (cell 3,6), and (cell 4,5). This occurs because the cells are arranged in two rows, separated by a cooling channel that maintains an initial temperature of 25 °C, which keeps the temperature values of neighbouring cells closely correlated and thermally balanced. The data also indicate that the r = 0.78 ratio results in a notable reduction in average temperatures relative to the other cases.

Furthermore, the thermal characteristics of all cells, regardless of the spacing ratio, exhibit similar behaviour because they are directly influenced by the liquid temperature in the cooling channel and the overall coolant distribution pattern. The behaviour of the average temperature curves further highlights the system's transient thermal response. During the early stages of discharge, the curves exhibit relatively steep gradients, indicating that the rate of heat generation within the cells exceeds the rate of heat dissipation to the coolant. As the process progresses, the slopes of the curves gradually decrease, reflecting the cooling system's increasing capacity to dissipate the heat generated by the battery cells, ultimately achieving a dynamic balance within the system. Among the configurations, r = 0.78 exhibits a faster flattening of the average temperature curve, suggesting more effective cooling performance and earlier stabilization. In contrast, r = 0.33 and r = 0 maintain steeper gradients for longer durations, implying reduced cooling efficiency and delayed thermal equilibrium.

The spacing ratio is therefore a critical factor not only in determining the final temperature uniformity of the battery module but also in governing the rate at which equilibrium is reached. At r = 0.78, the system demonstrates a superior ability to suppress temperature inhomogeneity and establish a more uniform and stable thermal distribution across all cells. In contrast, at r = 0.33, the temperature profile becomes less stable, resulting in more pronounced non-uniformities throughout the discharge process. When the spacing ratio r = 0, the absence of spacing results in significantly higher average temperatures, indicating a substantial reduction in cooling efficiency and a greater susceptibility to localized hot spots near the upper regions of the cells. These findings highlight that a strategic spacing configuration is not only effective at reducing peak and average temperatures but is also crucial for achieving homogeneous heat distribution, improved cooling stability, and faster thermal stabilization within the battery module.

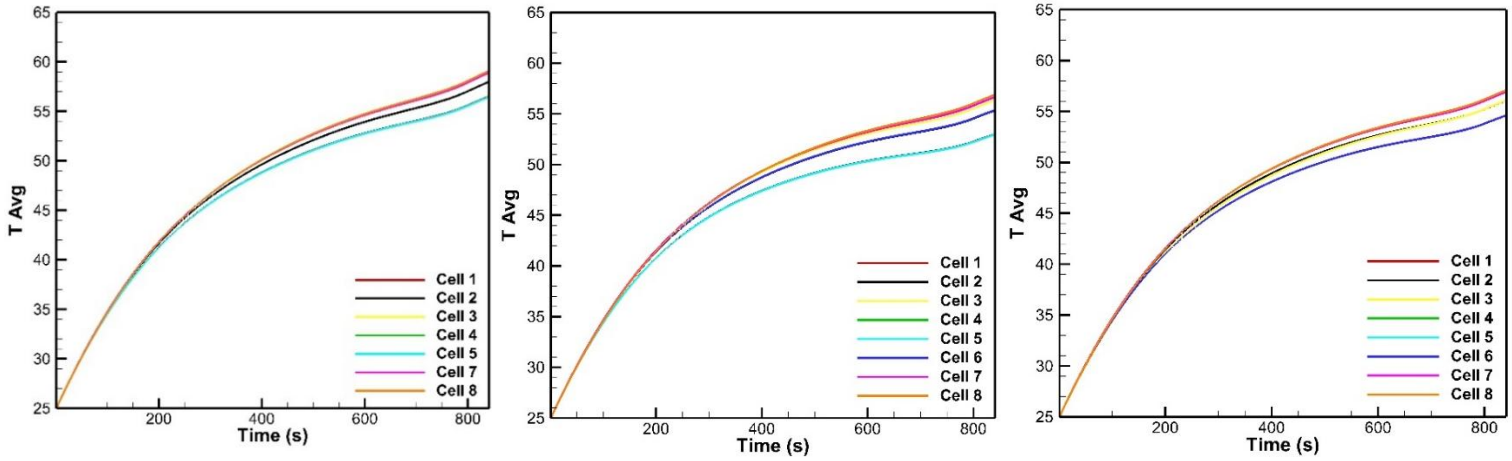

(a) (b) (c)

Fig. 7. Average temperature curves (a) r = 0.78, (b) r = 0.33, and (c) r = 0

3.2.2 Maximum temperature and uniformity

The evolution of the battery's maximum temperature across different spacing ratios is shown in Fig. 8. The results show that during the initial period (0–300 s), steep gradients across all spacing ratios indicate that the rate of heat generation within the cells exceeds the cooling system's heat-removal capacity. As the discharge process continues, the slopes of the curves gradually decrease, indicating that the cooling mechanism progressively compensates for the heat generated and guides the system toward dynamic equilibrium. Among the configurations examined, the r = 0.78 spacing exhibits a more rapid flattening of the curve, confirming that wider spacing improves cooling performance and accelerates stabilization. In contrast, the r = 0.33 configuration, and particularly r = 0, maintains steeper gradients for extended periods, suggesting that reduced spacing increases thermal resistance, restricts coolant flow, and delays the attainment of equilibrium. As shown in all figures, which present curves for all cells at various spacing ratios, the curves were identical, indicating that the spacing maintained the maximum temperature among the cells.

As time exceeds 300 s, slight differences between the curves begin to appear, but the deviation in T max among all battery cells remains small, with a difference of less than 2 °C. For r = 0.78, the temperature curves of all cells are nearly parallel throughout the simulation, differing only slightly, indicating a more uniform heat distribution. At r = 0.33, the differences become more pronounced with increasing flow time but remain within the 2 °C threshold. From the heat-reduction perspective, all variations perform similarly, with r = 0.78 showing a slight advantage over the others; from the uniformity perspective, r = 0.33 and r = 0 show greater heterogeneity. Overall, the results indicate that spacing variations in this range have a positive effect on thermal uniformity.

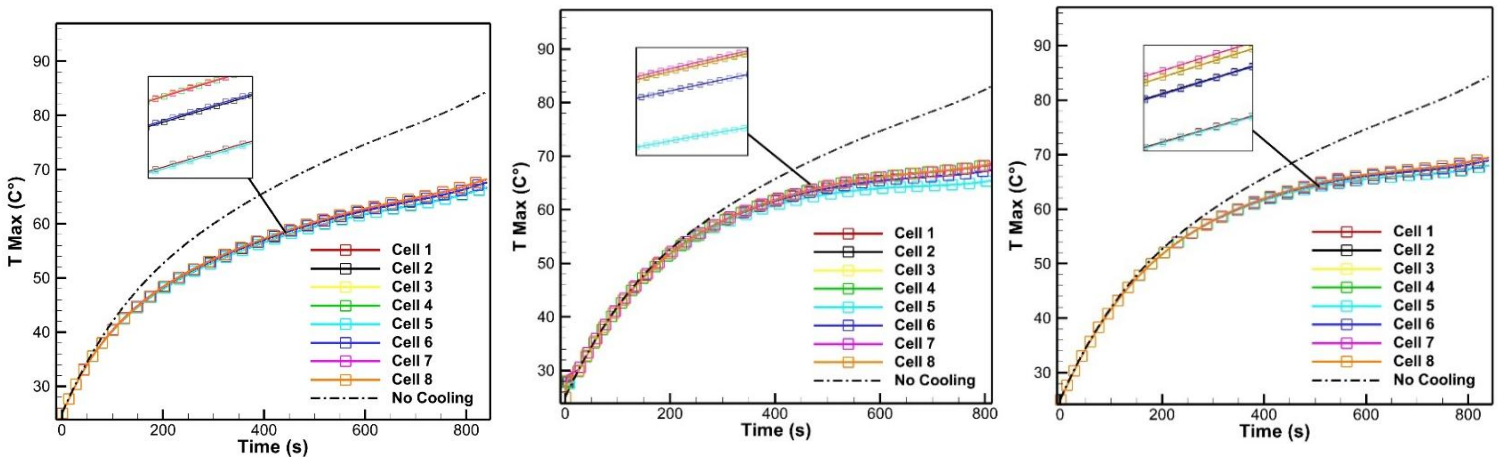

(a) (b) (c)

Fig. 8. Maximum temperature curves (a) r = 0.78, (b) r = 0.33, and (c) r = 0

Table 4. Heat reduction percentage

Cell	Without cooling	T Max reduction (%)		
		r = 0.78	r = 0.33	r=0
1	84.358°C	20.947	21.884	19.356
2		19.823	19.490	18.292
3		19.115	18.183	17.699
4		19.038	18.041	17.634
5		19.037	18.056	17.630
6		19.140	18.205	17.684
7		19.793	19.493	18.306
8		20.997	21.919	19.373
Average		19.736 %	19.409 %	18.247 %

During the discharge phase of a Li-ion battery cycle, each cell inherently generates heat due to internal chemical reactions and resistive losses, with the highest temperatures typically occurring at the maximum flow time, corresponding to the maximum discharge time. As shown in Table 4, the heat reduction percentage for each battery cell is calculated relative to the no-cooling condition, revealing that a spacing ratio of r = 0.78 consistently yields the highest average heat reduction across all cells, followed by r = 0.33 and r = 0. The observed pattern demonstrates that the spacing not only suppresses peak cell temperatures but also sustains more efficient thermal reduction across all cells throughout the discharge process, which is crucial for extending battery lifespan and maintaining performance stability under operational loads. In Fig. 9(a), with a spacing ratio r = 0.78, the temperature contours indicate that the cold plate provides the most significant cooling effect. The sections of the cylindrical battery cells that have direct and substantial contact with the cold plate, especially the top and bottom areas, display a significant reduction in temperature. This outcome indicates that conduction heat transfer from the battery cells to the cold plate is highly effective. Subsequent forced convection within the cold plate channels effectively removes heat from the circulating coolant. On the other hand, the interiors of cells not in direct contact with the cold plate continue to generate internal heat. In these regions, heat must first conduct through the cell's solid material before reaching the cooled surfaces. This slower process results in the localized areas of higher temperature, which are represented by darker regions on the contour map, highlighting the limitations of conduction when heat must travel over greater internal distances.

As the spacing ratio decreases to r = 0.33, as presented in Fig. 9(b), the contours reveal a more noticeable accumulation of heat. This increase in temperature is observed in the upper portions of the cells, near the positive pole, where a larger, darker high-temperature region forms. Smaller spacing reduces the available coolant flow path around the cells, thereby reducing the efficiency of convective cooling. In the configuration with r = 0, as illustrated in Fig. 9(c), where there is no spacing between adjacent cells, the temperature contours highlight an even more widespread and intense hot-spot region. The absence of spacing prevents the cooling effect of the cold plate from being effectively distributed across the entire cell surface. This arrangement leaves the upper areas of the cells particularly shielded from efficient cooling, resulting in greater heat accumulation there. Under these conditions, the primary mechanism of heat dissipation from the shielded areas is conduction through the battery material itself.

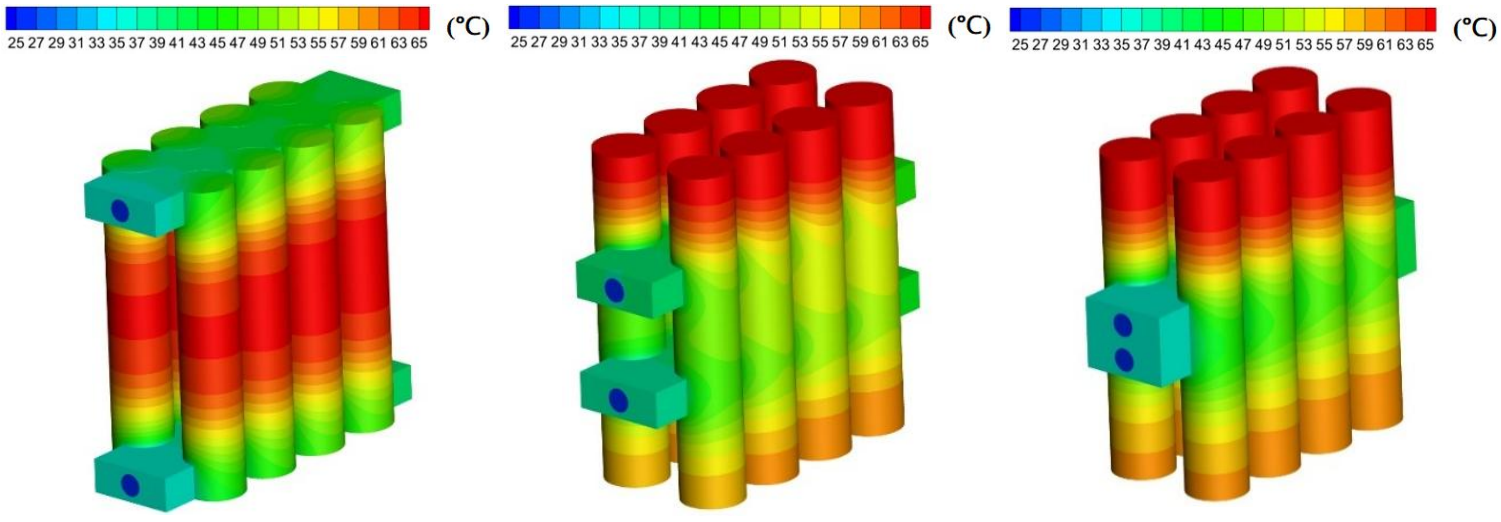

(a) (b) (c)

Fig. 9. Contour visualization (a) r = 078, (b) r = 0.33, and (c) r = 0

4 Conclusions

This study shows that varying the cold-plate spacing is crucial for improving the thermal performance of a cylindrical Li-ion 42110 battery pack. The cold plates lowered the maximum battery temperature compared to the no-cooling condition and helped maintain thermal uniformity across the module. The results indicate that r = 0.78 consistently yields the highest average heat reduction (19.736%), followed by r = 0.33 and r = 0, with a maximum deviation of 2% relative to the r = 0.78 value. The r = 0.78 configuration effectively minimizes localized hot spots and significantly reduces the temperature difference among cell regions, indicating optimal thermal spreading. The test conditions with r = 0.33 and r = 0 exhibit significantly larger temperature differences within and between the cells. Such temperature non-uniformity is a critical concern for battery performance, as it can accelerate degradation, reduce overall cycle life, and compromise safety by generating thermal stresses. The study also finds that, during the discharge phase at 5 °C, the spacing configuration directly influences heat dissipation, thereby maintaining a maximum temperature below that observed under no-cooling conditions. Despite the temperature contour analysis revealing that the upper regions of the battery remain the hottest due to reduced coolant exposure, the optimized cold plate configuration effectively suppresses excessive heat accumulation. These results confirm that cold plate spacing is a key parameter in balancing peak temperature reduction and uniform heat distribution, suggesting that further optimization of geometry and placement could lead to a more effective battery cooling system. This comprehensive heat-transfer analysis highlights that the spacing ratio is not merely a geometric parameter but a critical design variable for achieving a delicate balance between optimal thermal uniformity and effective peak-temperature control.

References

[1] S. Panchal, I. Dincer, M. Agelin-Chaab, R. Fraser, and M. Fowler, "Experimental and theoretical investigation of temperature distributions in a prismatic lithium-ion battery," *International Journal of Thermal Sciences*, vol. 99, pp. 204–212, 2016.

[2] X. Liu, C. Zhang, and J. Wu, "A novel temperature-compensated model for power Li-ion batteries with dual-particle-filter state of charge estimation," *Applied Energy*, vol. 123, pp. 263–272, 2014.

[3] S. Panchal, I. Dincer, M. Agelin-Chaab, R. Fraser, and M. Fowler, "Experimental and theoretical investigations of heat generation rates for a water cooled LiFePO4 battery," *International Journal of Heat and Mass Transfer*, vol. 101, pp. 1093–1102, 2016.

[4] R. Liu, J. Chen, J. Xun, K. Jiao, and Q. Du, "Numerical investigation of thermal behaviors in lithium-ion battery stack discharge," *Applied Energy*, vol. 132, pp. 288–297, 2014.

[5] P. Ping, Q. Wang, P. Huang, J. Sun, and C. Chen, "Thermal behaviour analysis of lithium-ion battery at elevated temperature using deconvolution method," *Applied Energy*, vol. 129, pp. 261–273, 2014.

[6] A. Greco, X. Jiang, and D. Cao, "An investigation of lithium-ion battery thermal management using paraffin/porous-graphite-matrix composite," *Journal of Power Sources*, vol. 278, 2015.

[7] M. K. Saudi, H. Hassan, A. S. G. Khalil, and M. Emam, "Thermal management of lithium-ion battery packs in electric vehicles using an innovative heat sink design," *International Journal of Thermal Sciences*, vol. 218, p. 110193, 2025.

[8] V. Saxena, S. K. Sahu, S. I. Kundalwal, and P. A. Tsai, "Optimizing battery thermal management with phase change materials: Influence of thickness, ambient conditions, and material selection," *Journal of Energy Storage*, vol. 132, p. 117657, 2025.

[9] S. W. Kim, H. W. Son, and D. R. Kim, "Enhanced cooling effect of core-shell phase change composite thin film on lithium-ion battery for delaying degradation," *International Communications in Heat and Mass Transfer*, vol. 169, p. 109530, 2025.

[10] S. Birinci *et al.*, "Effect of cooling plate contact area and flow rate on the performance of liquid-cooled cylindrical lithium-ion battery pack," *Applied Thermal Engineering*, vol. 279, p. 127708, 2025.

[11] Z. Rao, Z. Qian, Y. Kuang, and Y. Li, "Thermal performance of liquid cooling based on thermal management system for cylindrical lithium-ion battery module with variable contact surface," *Applied Thermal Engineering*, vol. 123, pp. 1514–1522, 2017.

[12] S. Aftab, A. Rafie, N. Razak, and K. Ahmad, "Turbulence Model Selection for Low Reynolds Number Flows," *PLoS One*, vol. 11, p. e0153755, 2016.

[13] Z. Zhang and K. Wei, "Experimental and numerical study of a passive thermal management system using flat heat pipes for lithium-ion batteries," *Applied Thermal Engineering*, vol. 166, p. 114660, 2020.

[14] C. Wang *et al.*, "Liquid cooling based on thermal silica plate for battery thermal management system," *International Journal of Energy Research*, vol. 41, 2017.

[15] Z. Wang, J. Ma, and L. Zhang, "Finite Element Thermal Model and Simulation for a Cylindrical Li-Ion Battery," *IEEE Access*, pp. 1–1, 2017.

[16] X. Peng, C. Ma, A. Garg, N. Bao, and X. Liao, "Thermal performance investigation of an air-cooled lithium-ion battery pack considering the inconsistency of battery cells," *Applied Thermal Engineering*, vol. 153, pp. 596–603, 2019.

[17] P. J. Roache, "Perspective: A Method for Uniform Reporting of Grid Refinement Studies," *Journal of Fluids Engineering*, vol. 116, pp. 405–413, 1994.

[18] Z. Rao, Y. Huo, X. Liu, and G. Zhang, "Experimental investigation of battery thermal management system for electric vehicle based on paraffin/copper foam," *Journal of the Energy Institute*, vol. 88, pp. 241–246, 2015.

[19] P. J. Roache, "Perspective: A Method for Uniform Reporting of Grid Refinement Studies," *Journal of Fluids Engineering*, vol. 116, pp. 405–413, 1994.

[20] Z. Rao, Y. Huo, X. Liu, and G. Zhang, "Experimental investigation of battery thermal management system for electric vehicle based on paraffin/copper foam," *Journal of the Energy Institute*, vol. 88, pp. 241–246, 2015.